ACS APPLIED MATERIALS & INTERFACES

Letter

www.acsami.org

Layered Tantalum Oxynitride Nanorod Array Carpets for Efficient Photoelectrochemical Conversion of Solar Energy: Experimental and DFT Insights

Nageh K. Allam,* Basamat S. Shaheen, and Ahmed M. Hafez

Energy Materials Laboratory (EML), Physics Department, School of Sciences and Engineering, The American University in Cairo, New Cairo 11835, Egypt

Supporting Information

ABSTRACT: Anodically fabricated tantalum oxide (Ta_2O_5) nanorod array carpets are converted into the corresponding tantalum oxynitride (TaON) through nitridation in an ammonia atmosphere. The measured optical bandgap energy of TaON is ~2.3 eV, which is also confirmed via the density functional theory calculations. When used to photoelectrochemically split water (AM 1.5G illumination, 1 M KOH, and 0.6 V applied DC bias), the multilayer nanorod films show visible-light incident photon conversion efficiencies (IPCE) as high as 7.5%. The enhanced photochemical activity is discussed in terms of the ordered one-dimensional morphology as well as the electron effective mass in TaON and Ta_2O_5.

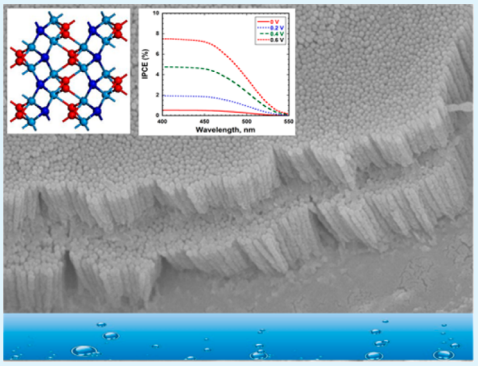

KEYWORDS: *oxynitride, solar, hydrogen, DFT, effective mass, nanorods*

Despite the enormous efforts over the past decades to design and develop functional materials for hydrogen production via solar water splitting, no known system currently meets the requirements for a commercially viable solar-hydrogen process. The long-standing bottleneck is the fact that the majority of photocorrosion stable materials are wide band gap metal oxides, with limited absorption activity to the ultraviolet spectral region, which contains only about 3-5% of the incident solar energy. With the progress in the nano-fabrication techniques, the nanoscale control of such metal oxides can enhance their optical and structural properties, rendering such nanostructured materials useful in a plethora of applications, including the solar energy conversion. The nano-structured metal oxide systems demonstrated to date are still limited by the minimal visible light absorption,[1] which can be explained by following the early work of Scaife.[2] Scaife noted that the valence bands of oxide semiconductor materials are mainly formed by O 2p orbitals, the levels are fixed at a highly positive level of around 3.0 V versus the normal hydrogen electrode (NHE). Moreover, the oxides that have narrow band gaps (<3.0 eV), such as Fe_2O_3 and WO_3, are either unstable or do not have the right band alignment required for water splitting, and therefore require a large external bias.[2]

Because of the high potential energy of the metal−nitrogen bond compared to the metal−oxygen bond,[3] transition metal oxynitrides[3−7] have been identified as an alternative class of materials that can efficiently be used for solar energy conversion processes. This difference in bond energy resulted in narrower band gap energies in oxynitrides compared to their metal oxide counterparts. In addition, oxynitrides are ideal photoelectrodes for water splitting applications because of their stability in alkaline media.[3−7]

Among all studied oxynitrides, tantalum oxynitride (TaON) showed a great promise as a visible-light responsive photo-electrode with suitable band-edge positions for water splitting.[8,9] However, most of the reported TaON materials are in the form of either powders or thin films. Powders are not practical for a scalable photolysis process. Also, with thin films, the light absorption and carrier collection are in competition, i.e., although thick films are needed to harvest a reasonable amount of the solar spectrum, thicker films than the carrier diffusion length (usually tens of nanometers) will result in poor carrier collection efficiency.[10]

In 2008, Allam et al.[11] first reported the ability to grow well-aligned Ta_2O_5 nanotube arrays by a simple but optimized anodization of a tantalum metal. This report triggered intense research activities to study the properties and applications of such nanotube arrays.[12−16] For example, Banerjee et al.[17] reported the synthesis of TaON nanotube arrays for visible light-driven photoelectrochemical generation of hydrogen from water. Under AM 1.5 G conditions, the fabricated TaON NTs showed a photocurrent density of 2.6 mA/cm^2 at 0.5 $V_{Ag/AgCl}$. The visible light contribution of the TaON NTs photocatalyst was estimated to be around 47% of its activity under AM 1.5

Received: January 16, 2014
Accepted: March 25, 2014
Published: March 25, 2014

   dx.doi.org/10.1021/am500286n | ACS Appl. Mater. Interfaces 2014, 6, 4609−4615

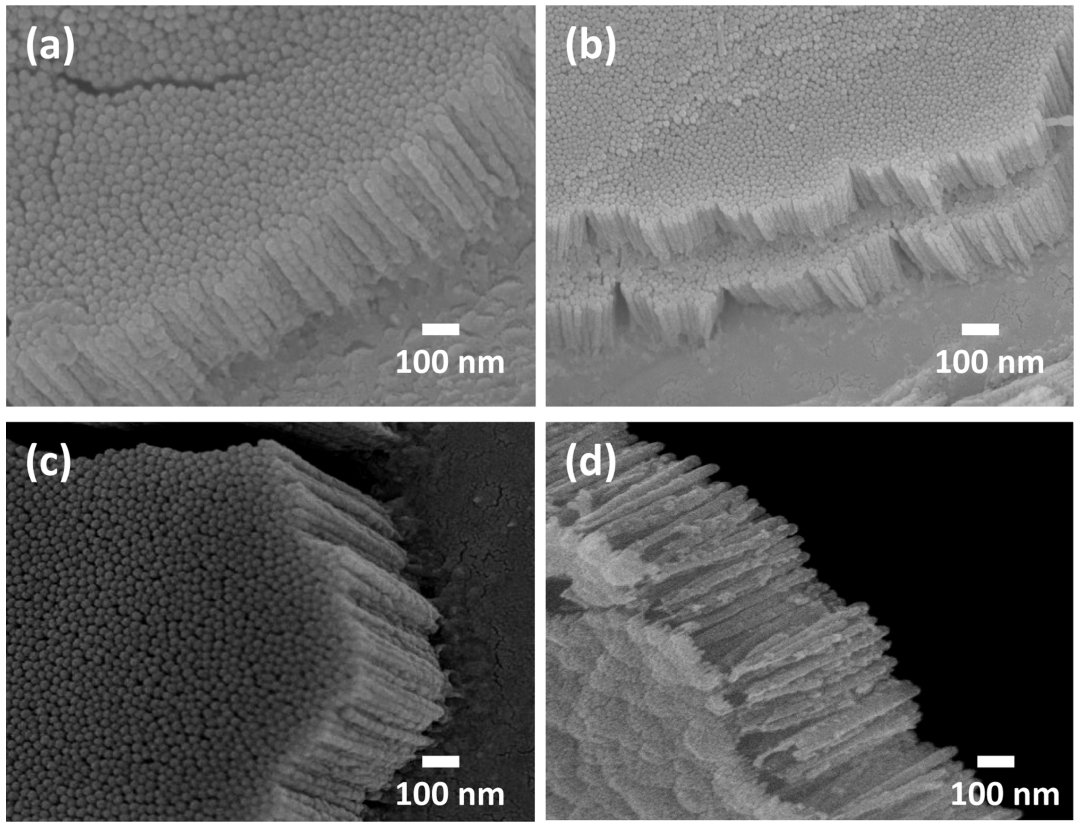

Figure 1. FESEM images of the nanorod arrays. Panels a and b are images of the as-anodized single and multi-layerd tantalum oxide nanorod films, respectively. Panels c and d are images of the nanorod films annealed in ammonia atmosphere for 6 h at 550 and 600 °C, respectively.

irradiation, which is quite significant compared to metal oxide nanotubes.[17] Feng et al.[18] reported the fabrication of highly oriented Ta_3N_5 nanotube array films with a band gap of 2.07 eV, enabling the collection of more than 45% of the incident solar spectrum energy. Using 0.5 V dc bias under AM 1.5 illumination, a 240 nm sample showed a visible light IPCE of 5.3%.

Herein, we report the first demonstration of the fabrication of vertically aligned tantalum oxynitride nanorod arrays and their use for solar water splitting. The nanorod architecture with a thin lateral thickness is expected to facilitate the diffusion of the photogenerated holes to the semiconductor/electrolyte interface during water splitting, especially when this thickness is within the minority carrier diffusion length, allowing for efficient separation of charge carriers.

The fabrication of tantalum oxynitride nanorod arrays involved two consecutive steps; anodization and nitridation. The anodization step is detailed elsewhere.[11] The nitridation step involved the annealing of the as-anodized samples in a NH_3 atmosphere (200 sccm) at different temperatures. The DFT calculations were performed under local density approximation (LDA) with the Ceperley-Alder form[19] using the CASTEP code (plane-wave pseudopotential method).[20] For structure optimization and energy calculation, the convergence criteria were set to k-point meshes of 7 × 7 × 7 and a kinetic energy cut-off of 800 eV for tantalum oxynitride. Geometry optimization was performed for the atomic positions while the lattice parameters were kept fixed, followed by single point energy calculations. The accuracy of self-consistent convergence was set at 5.0×10^{-6} eV/atom. The convergence criterion for the maximal force between atoms was 0.01 eV/A with the maximum displacement was used as 5.0×10^{-4} Å, and the stress was 0.02 GPa. The densities of state (DOS), electronic band structures, and optical properties were also investigated using the optimized structures. The effective mass calculations have been done using DFT under the LDA for the exchange correlation function, as implemented in the ABINIT package.[21,22] For all chemical elements, projected-augmented wave pseudo-potentials with electronic wave function plane-waves truncated at about 400 eV (15 Ha) were used. The Brillouin zone integrations were done on 4 × 4 × 4 k-point Monkhorst-Pack grids and all structural optimizations were performed until atomic forces were smaller than 0.5 meV/ Å. Band masses were extracted using the ABINIT package from the inverse of the second derivative at the two conduction band minima with k points spacing of Δk = 0.001 along the high symmetry directions Γ-Y, Γ -Z, B-A, and B-D up to one-fifth of the distance from Γ to the zone boundaries Y and Z and up to two-fifth the distance from B to the zone boundaries A and D.[23] We found this distance sufficient to get parabolic conduction bands around the minima, and to neglect the effects of band non-parabolicity.

We previously showed that the anodization of tantalum in stirred mixtures of concentrated HF and H_2SO_4 (1:9 to 2:8 ratios) resulted in the formation of nanodimpled tantala surfaces.[11] Herein, we investigated the effect of the addition of EG to the anodization electrolyte to achieve stable and ordered tantalum oxide nanostructures, based on the previous reports for the anodization of many valve metals.[23−27] Figure 1a shows the formation of well-aligned nanorod arrays, with thicknesses up to 600 nm, upon the anodization of tantalum for 20 min at 10 V in aqueous electrolytes of 1:9 HF+H_2SO_4 and containing

5 vol % EG. More interestingly is that the anodization of tantalum, under the same applied voltage, in the previously used electrolyte resulted in the formation of multilayer tantalum oxide nanorod arrays (Figure 1b) with the thickness of each layer being ∼350 nm. We noticed that Macak et al.[28] reported a two-step anodization method for the formation of multilayer TiO_2 nanotube arrays in glycerol/NH_4F mixtures. They related the growth of the second layer to the formation of narrow channels in the early stages of the anodization process. It is worth noting that anodization at 20 V resulted in the detachment of the formed nanorod layers.

Images c and d in Figure 1 are FESEM images of the annealed nanorod arrays in ammonia ambient at 550 and 600 °C, respectively. In contrast to the conventional aggregation of tantalum oxide nanoparticles upon their annealing at high temperature,[29] the nanorod morphology was preserved despite the high-temperature nitridation process. However, it is worth mentioning that the conversion of tantalum oxide into tantalum oxynitride occurs only in a very narrow window of annealing conditions. As both oxides and oxynitrides have virtually overlapping X-ray diffraction patterns,[30,31] X-ray photoelectron spectroscopy (XPS) is considered the most powerful technique for the distinction between oxynitrides and oxides. For example, XPS analysis of the nanorods annealed at temperatures below 600 °C (not shown) revealed two peaks characteristic of energy losses[32] (at 398.9 eV) or adsorbed NH_x species[6,33] (at 400.7 eV). Figure 2a shows the XPS spectra of a nanorod film annealed in ammonia atmosphere at 600 °C for 6 h. The inset in Figure 2a shows the photoemission spectra of Ta 4p and N 1s. Note that the photoemission line for N 1s appears at ∼396 eV characteristic for tantalum oxynitride.[6,34] The oxynitride nanorods were further characterized via the nano-beam diffraction (NBD) and transmission electron diffraction (TED) patterns, Figure 2b, confirming the crystallization and formation of oxynitride upon nitridation.

Figure 2c shows the ultraviolet-visible diffuse reflectance spectra (UV−vis DRS) of the tantalum oxynitride single and multilayer nanorod films annealed at 600 °C in ammonia atmosphere for 6 h, along with tantalum oxide nanorods film annealed at the same temperature but in O_2 ambient for comparison. The absorption intensity of the multilayer (m-TaON) nanorod film is higher than that of the single-layer (s-TaON) film, which can be related to the difference in film thickness. Typically, an extrapolated line from the absorption edge to the energy axis is drawn to determine the bandgap values. The absorption edges of the m-TaON and s-TaON are located at approximately 540 and 530 nm, respectively. These absorption edges are red shifted by ∼240 nm from that of the Ta_2O_5 nanorod array film, resulting in bandgap energy (E_g) in the range 2.3 to 2.34 eV. The valence and conduction bands of tantalum oxynitride are attributed to the N 2p and Ta 5d orbitals, respectively. As the potential energy of the N 2p orbitals is higher than that of O 2p, the substitution of N for O is expected to result in a valence band of higher negative potential and narrowing of the band gap of the tantalum oxynitrides compared to their oxide counterparts.[29]

To have more insights into the optical and structural properties of the tantalum oxynitride, we have performed density functional theory (DFT) calculations on the structure shown in Figure 3a. Tantalum oxynitride is an indirect bandgap semiconductor with a bandgap of 2.08 eV. However, at the highly symmetric G point (Figure 3b), tantalum oxynitride shows a direct bandgap of 2.4 eV, which is very close to the

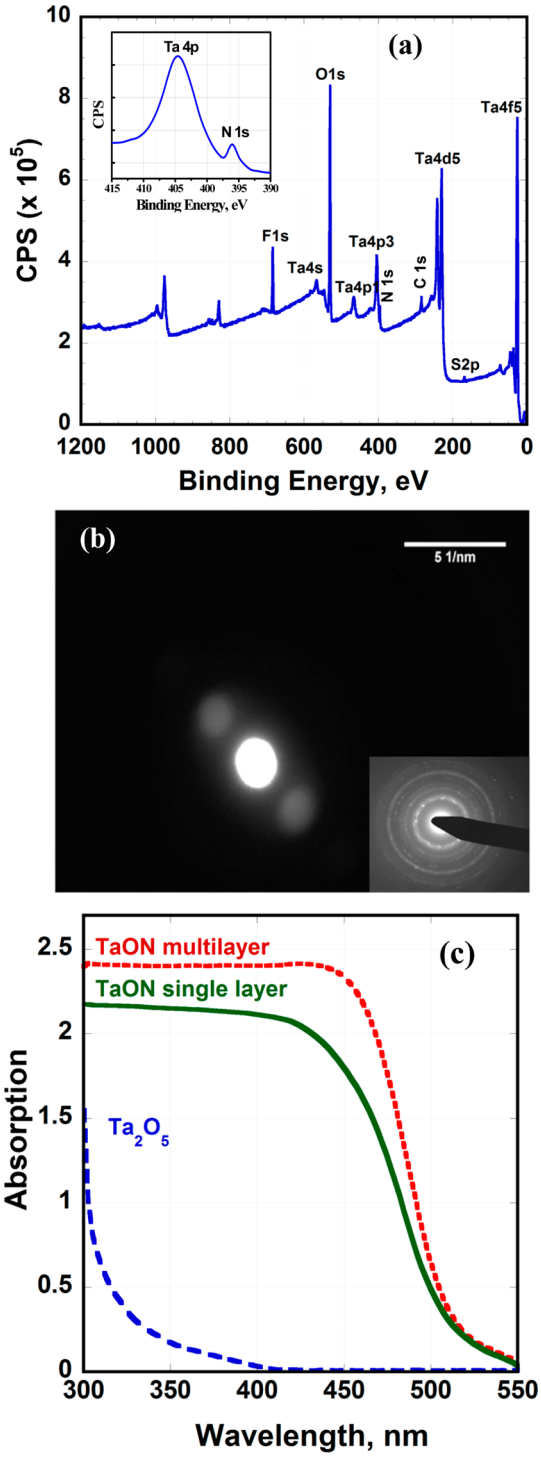

Figure 2. (a) X-ray photoemission spectra, (b) nano-beam diffraction (NBD) and transmission electron diffraction (TED) of the nanorod array film annealed in ammonia atmosphere at 600°C for 6 h, and (c) the diffuse reflectance UV−vis spectra of the nanorod array films. The Ta_2O_5 film was obtained by annealing the as anodized tantalum oxide at 600 °C for 6 h in oxygen ambient, whereas the TaON films were obtained by annealing the as-anodized single and multilayer films at 600 °C for 6 h in ammonia atmosphere.

bandgap, estimated from the DRS measurements shown in Figure 2c. From the total and partial density of states of the tantalum oxynitride (Figure 3c), the states lying in the energy range −15.2 to −12.4 eV are contributed by the N 2s states

dx.doi.org/10.1021/am500286n | ACS Appl. Mater. Interfaces 2014, 6, 4609−4615

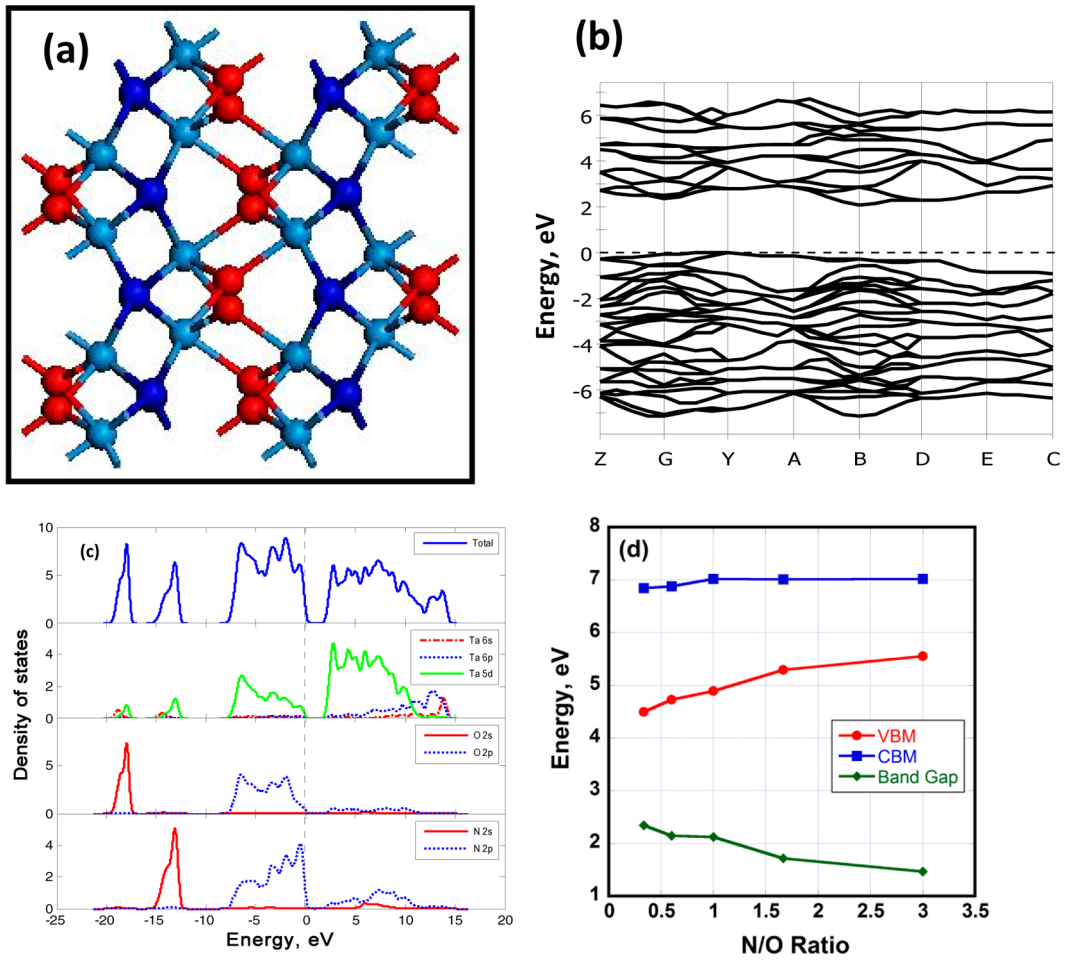

Figure 3. (a) Crystal structure of TaON (light blue, red, and dark blue colors represent Ta, O, and N atoms, respectively) and the corresponding (b) electronic band structure, (c) total and partial density of states, and (d) the variation of VBM, CMB, and bandgap energies of the material as a function of N/O ratio.

with contributions from the Ta d−s−p hybridized states. However, the states appear in the energy range −19 to −17 eV originate from the O 2s states with less contribution from the Ta d−s−-p hybridized orbitals. Note that the partial density of states (PDOS) in the range of approximately −7.6 to 0 eV indicate the potential covalent bonding character in tantalum oxynitride as they mainly stem from the contribution of N 2p, O 2p, and Ta 5d orbitals. A dispersion in the valence band maximum, raising it up (as it is dominated by the N 2p states), may be observed as a result of such covalent character, which can be held responsible for the observed bandgap narrowing and visible light response of tantalum oxynitride.

Further, DFT was used to investigate the effect of the N/O ratio on the VBM and CBM positions and consequently on the resulted bandgap of the material, see Table S1 in the Supporting Information and Figure 3d. Increasing the N/O ratio resulted in an increase in the valence band energy without a noticeable shift in the position of the conduction band edge. The insensitivity of the conduction band to the N/O ratio may indicate the least contribution of the N or O 2p states to the bottom of the CBM, confirming that the change in the VBM position is the main reason for the observed bandgap narrowing. Our results are in agreement with those reported by Chun et al.[29] using electrochemical and ultraviolet photoelectron spectroscopy (UPS) measurements confirming the shift in the VBM to higher energies in the order Ta_2O_5 < TaON < Ta_3N_5, with similar CBM positions. The decrease in the bandgap (from ∼2.3 to ∼1.5 eV) with increasing the N/O ratio (from 2/6 to 6/2), see Table S1 in the Supporting Information, can be attributed to the variation in the number of valence electrons.

The water photoelectrolysis test using the fabricated tantalum oxynitride photoanodes was carried out in a three-electrode electrochemical cell in a 1.0 M KOH electrolyte solution, Figure 4a. Negligible current densities (∼50 $\mu A/cm^2$) were observed under dark conditions. Upon illumination (AM 1.5, 100 mW/cm^2), a significant increase in the photocurrent was observed, indicating good charge carriers transport and network forming ability of the nanorod electrodes. The high photocurrent-to-dark current ratio implies that the majority of the photocurrent is generated only by absorbed photons with no dark-current contribution. The maximum obtained photocurrent densities were 3 mA cm^{-2} and 3.15 mA cm^{-2} for the single-layered and multi-layered tantalum oxynitride nanorod electrodes, respectively. Note that these values are higher than those reported for tantalum oxynitride nanotubes (2.6 mA cm^{-2}).[16] Also, the onset potential (−1.17 $V_{Ag/AgCl}$), the light contribution toward the minimum potential needed for water splitting process to take place,[35] is more negative than that shown for tantalum oxynitride nanotubes (−1.0 $V_{Ag/AgCl}$).[16] Therefore, the nanorod photoanodes require less voltage for

dx.doi.org/10.1021/am500286n | ACS Appl. Mater. Interfaces 2014, 6, 4609−4615

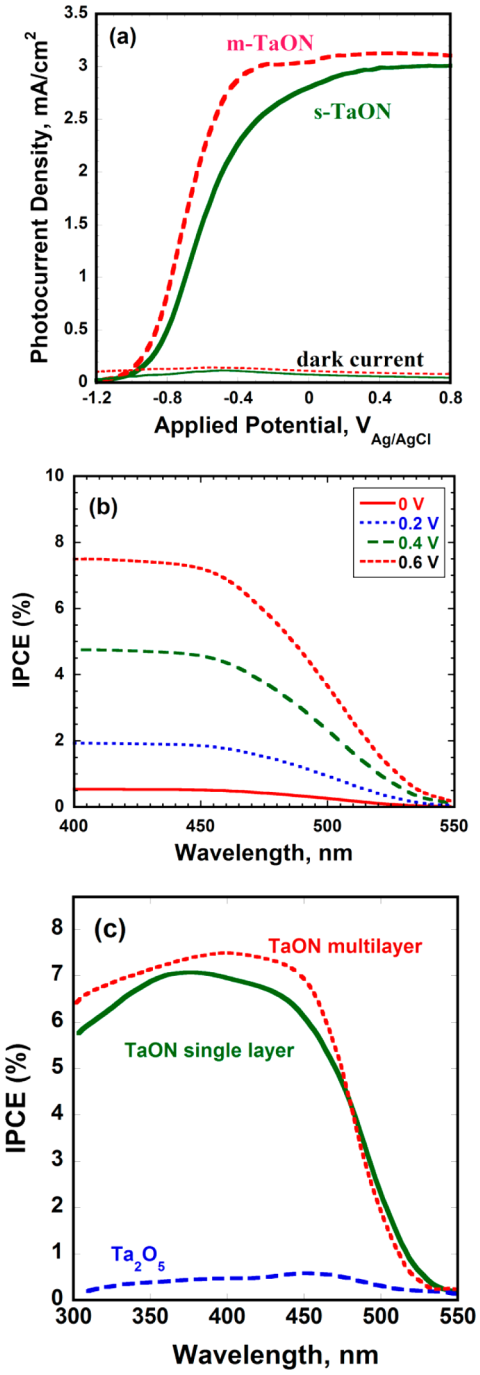

Figure 4. (a) Photocurrent density versus applied potential in 1 M KOH aqueous solution under AM 1.5 illumination for the single-layered and multi-layered tantalum oxynitride electrodes with a scan rate of 10 mV/s, (b) the IPCE plots of multi-layered TaON nanorod films in 1 M KOH aqueous solutions under different applied voltages, and (c) the corresponding IPCE values for tantalum oxide and tantalum oxynitride nanorod array films under an applied dc potential of 0.6 V.

water oxidation than the nanotube photoanodes counterparts, indicating more favorable photoelectrochemical activity.

The incident photon conversion efficiency (IPCE) experiments were performed in a two-electrode arrangement with the TaON nanorod array film as the working photoelectrode and platinum foil as a counter electrode in 1.0 M KOH solution. Figure 4b shows the obtained IPCE for the multi-layered tantalum oxynitride (m-TaON) nanorod array films as a function of the irradiation wavelength under different applied potentials. The IPCE was calculated using eq 1, where λ is the wavelength of incident light, i_{ph} is the photocurrent density under illumination at λ and I_o is the incident light intensity at λ.

$$\text{IPCE\%} = \frac{(1240\ \text{eV nm})(i_{ph}\ \text{mA cm}^{-2})}{(\lambda\ \text{nm})(I_o\ \text{mW cm}^{-2})} \times 100 \quad (1)$$

The obtained IPCE values in the wavelength range from 400 to 550 nm indicate the activity of TaON films in the visible light, in accordance with the absorption spectra shown in Figure 3. The applied bias assists the separation of the photogenerated charge carriers, thereby enhancing the IPCE. Upon the use of 0.6 V, m-TaON film showed an IPCE value as high as ~7.5% over the wavelength range of 400−450 nm, after which it declines indicating that the photocurrent occurs as a result of the band gap transition. Based on this finding, we tested the s-TaON, m-TaON, and Ta_2O_5 nanorod array films in 1M KOH under 0.6 V applied dc bias in a two-electrode arrangement with the oxynitride nanorod film as the working photoelectrode and platinum foil as a counter electrode, Figure 4c. In general, the obtained IPCE for m-TaON and s-TaON nanorod films are almost the same with minor differences. However, those IPCE values are much greater than that obtained for the pristine Ta_2O_5 nanorod film, in good agreement with the UV−vis DRS results shown in Figure 2c. We note that our obtained IPCE of 7.5% is higher than that reported for tantalum nitride nanotube arrays, in agreement with Domen et al.[9] who showed TaON powders to have much higher IPCE values than the Ta_3N_5 counterparts. This high IPCE can also be supported by the calculated electron effective mass (m^*) of TaON at the gamma point ($m^* = 0.33m_o$) as compared to that reported[36,37] for pure Ta_2O_5 ($m^* = 0.5-0.7m_o$). The small effective mass of TaON implies small inertia or high mobility of electrons in TaON ($\mu = e\tau_s/m^*$), explaining the obtained high IPCE for TaON. However, unlike the UV−vis DRS results, the IPCE of the s-TaON is slightly higher than that of the m-TaON films at wavelengths greater than 500 nm. This can be related to the larger thickness of the m-TaON films compared to the s-TaON. In this case, the electrons will need to travel longer distance in the m-TaON to reach the back contact, which may cause an increase in charge carriers' recombination. Recently, there are some reports on the possibility to suppress surface defect formation during nitridation through the addition of either cobalt[35,38,39] or zirconium[40] oxides. However, it should be noted that our results (IPCE of ~7%) are much greater than those reported for N-doped TiO_2 (IPCE of ~0.4%),[41] N-doped WO_3 (IPCE of ~0.4%)[42] and NbON (IPCE of ~1%). Also, note that the thickness of the tested electrodes in our study is only 300 nm, with further improvements expected with thicker films. Because of their visible light activity and suitable band edges positions, the fabricated tantalum oxynitride nanorods can be a potential material architecture for water splitting.[29]

In conclusion, we report the first demonstration on a facile method for the fabrication of vertically oriented tantalum oxynitride nanorod array carpets via the anodization of tantalum, followed by nitridation of the resulting films. The morphology of the formed nanorod array films, either single or double layer, depends on the anodization conditions. The as-anodized nanorod array films showed exceptional stability upon their annealing in ammonia atmosphere up to 700 °C for 6 h, with the opportunity to convert Ta_2O_5 into TaON at

temperatures as low as 600 °C. This temperature is lower than that previously reported for Ta_2O_5 nanoparticles and without any observed structural aggregation/collapse. The optimized morphological (1D) and enhanced optical properties make TaON nanorods a potential candidate for visible light-driven water photoelectrolysis. The absorption edge is red shifted by ~240 nm from that of the Ta_2O_5 nanorod array film, resulting in a band gap energy of ~2.3 eV. This enhancement in the absorption characteristic as well as the bandgap narrowing is also confirmed via the density functional theory (DFT) calculations. The covalent character of Ta−O and Ti−N bonds results in a large dispersion in the valence band maximum raising it up, which can be held responsible for the observed bandgap narrowing and visible light response of TaON. IPCE values as high as 7.5% were achieved upon 0.6 V bias in 1 M KOH solution. The effective mass calculations show the higher electron mobility in TaON compared to that in Ta_2O_5 counterpart. We are currently investigating means for more precise control of the nitridation process and functionalization of the nanorods to reduce surface defects and increase the photoconversion efficiency.

■ ASSOCIATED CONTENT

Supporting Information

Supporting Information includes the variation of the VBM, CBM and bandgap energies as a function of the N/O ratio (Table S1). This material is available free of charge via the Internet at http://pubs.acs.org/.

■ AUTHOR INFORMATION

Corresponding Author

*E-mail: nageh.allam@aucegypt.edu.

Notes

The authors declare no competing financial interest.

■ ACKNOWLEDGMENTS

The financial support from The American University in Cairo is highly appreciated.

■ REFERENCES

(1) Jiang, Z.; Tang, Y.; Tay, Q.; Zhang, Y.; Malyi, O. I.; Wang, D.; Deng, J.; Lai, Y.; Zhou, H.; Chen, X.; Dong, Z.; Chen, Z. Understanding the Role of Nanostructures for Efficient Hydrogen Generation on Immobilized Photocatalysts. *Adv. Energy Mater.* **2013**, *3*, 1368−1380.

(2) Scaife, D. E. Oxide Semiconductors in Photoelectrochemical Conversion of Solar Energy. *Sol. Energy* **1980**, *25*, 41−54.

(3) Hitoki, G.; Takata, T.; Kondo, J. N.; Hara, M.; Kobayashi, H.; Domen, K. (Oxy) nitrides as New Photocatalysts for Water Splitting Under Visible Light Irradiation. *Electrochemistry* **2002**, *70*, 463−465.

(4) Maeda, K.; Teramura, K.; Saito, N.; Inoue, Y.; Kobayashi, H.; Domen, K. Overall Water Splitting Using (Oxy)nitride Photocatalysts. *Pure Appl. Chem.* **2006**, *78*, 2267−2276.

(5) Hu, C.-C.; Teng, H. Gallium Oxynitride Photocatalysts Synthesized from $Ga(OH)_3$ for Water Splitting under Visible Light Irradiation. *J. Phys. Chem. C* **2010**, *114*, 20100−20106.

(6) Allam, N. K.; Poncheri, A. J.; El-Sayed, M. A. Vertically Oriented Ti−Pd Mixed Oxynitride Nanotube Arrays for Enhanced Photoelectrochemical Water Splitting. *ACS Nano* **2011**, *5*, 5056−5066.

(7) Fuertes, A. Chemistry and Applications of Oxynitride Perovskites. *J. Mater. Chem.* **2012**, *22*, 3293−3299.

(8) Abe, R.; Higashi, M.; Domen, K. Facile Fabrication of an Efficient Oxynitride TaON Photoanode for Overall Water Splitting into H_2 and O_2 under Visible Light Irradiation. *J. Am. Chem. Soc.* **2010**, *132*, 11828−11829.

(9) Higashi, M.; Domen, K.; Abe, R. Fabrication of Efficient TaON and Ta_3N_5 Photoanodes for Water Splitting under Visible Light Irradiation. *Energy Environ. Sci.* **2011**, *4*, 4138−4147.

(10) Choi, K.S. Shape Effect and Shape Control of Polycrystalline Semiconductor Electrodes for Use in Photoelectrochemical Cells. *J. Phys. Chem. Lett.* **2010**, *1*, 2244−2250.

(11) Allam, N. K.; Feng, X. J.; Grimes, C. A. Self-Assembled Fabrication of Vertically Oriented Ta_2O_5 Nanotube Arrays, and Membranes Thereof, by One-Step Tantalum Anodization. *Chem. Mater.* **2008**, *20*, 6477−6481.

(12) El-Sayed, H. A.; Birss, V. I. Controlled Interconversion of Nanoarray of Ta Dimples and High Aspect Ratio Ta Oxide Nanotubes. *Nano Lett.* **2009**, *9*, 1350−1355.

(13) Barton, J. E.; Stender, C. L.; Li, P.; Odom, T. W. Structural Control of Anodized Tantalum Oxide Nanotubes. *J. Mater. Chem.* **2009**, *19*, 4896−4898.

(14) El-Sayed, H. A.; Birss, V. I. Controlled Growth and Monitoring of Tantalum Oxide Nanostructures. *Nanoscale* **2010**, *2*, 793−798.

(15) Ruckh, T.; Porter, J.R.; Allam, N.K.; Feng, X.J.; Grimes, C.A.; Popat, K.C. Nanostructured Tantala as a Template for Enhanced Osseointegration. *Nanotechnology* **2009**, *20*, 045102.

(16) Gonçalves, R.V.; Migowski, P.; Wender, H.; Eberhardt, D.; Weibel, D.E.; Sonaglio, F. C.; Zapata, M. J. M.; Dupont, J.; Feil, A. F.; Teixeira, S. R. Ta_2O_5 Nanotubes Obtained by Anodization: Effect of Thermal Treatment on the Photocatalytic Activity for Hydrogen Production. *J. Phys. Chem. C* **2012**, *116*, 14022−14030.

(17) Banerjee, S.; Mohapatra, S. K.; Misra, M. Synthesis of TaON Nanotube Arrays by Sonoelectrochemical Anodization Followed by Nitridation: A Novel Catalyst for Photoelectrochemical Hydrogen Generation from Water. *Chem. Commun.* **2009**, 7137−7139.

(18) Feng, X. J.; LaTempa, T. J.; Basham, J. I.; Mor, G. K.; Varghese, O. K.; Grimes, C.A. Ta_3N_5 Nanotube Arrays for Visible Light Water Photoelectrolysis. *Nano Lett.* **2010**, *10*, 948−952.

(19) Ceperley, D. M.; Alder, B. J. Exchange-Correlation Potential and Energy for Density-Functional Calculation. *Phys. Rev. Lett.* **1980**, *45*, 567−581.

(20) Segall, M.D.; Lindan, P. J. D.; Probert, M. J.; Pickard, C. J.; Hasnip, P. J.; Clark, S. J.; Payne, M.C. First-Principles Simulation: Ideas, Illustrations and the CASTEP Code. *J. Phys.: Condens. Matter* **2002**, *14*, 2717.

(21) Marques, M.; Teles, L. K.; Anjos, V.; Scolfaro, L. M. R.; Leite, J. R.; Freire, V. N.; Farias, G. A.; da Silva, E. F. Full-Relativistic Calculations of the $SrTiO_3$ Carrier Effective Masses and Complex Dielectric Function. *Appl. Phys. Lett.* **2003**, *82*, 3074.

(22) Bistritzer, R.; Khalsa, G.; MacDonald, A. H. Electronic Structure of Doped d^0 Perovskite Semiconductors. *Phys. Rev. B* **2011**, *83*, 115114.

(23) Howarth, L. E.; Gilbert, J. F. Determination of Free Electron Effective Mass of n-Type Silicon. *J. Appl. Phys.* **1963**, *34*, 236−237.

(24) Allam, N. K.; Grimes, C.A. Electrochemical Fabrication of Complex Copper Oxide Nanoarchitectures *via* Copper Anodization in Aqueous and Non-Aqueous Electrolytes. *Mater. Lett.* **2011**, *65*, 1949−1955.

(25) Yang, Y.; Albu, S.P.; Kim, D.; Schmuki, P. Enabling the Anodic Growth of Highly Ordered V_2O_5 Nanoporous/Nanotubular Structures. *Angew. Chem., Int. Ed.* **2011**, *50*, 9071−9075.

(26) LaTempa, T. J.; Feng, X.; Paulose, M.; Grimes, C. A. Temperature-Dependent Growth of Self-Assembled Hematite (α-Fe_2O_3) Nanotube Arrays: Rapid Electrochemical Synthesis and Photoelectrochemical Properties. *J. Phys. Chem. C* **2009**, *113*, 16293−16298.

(27) Allam, N. K.; Shankar, K.; Grimes, C.A. A General Method for the Anodic Formation of Crystalline Metal Oxide Nanotube Arrays without the Use of Thermal Annealing. *Adv. Mater.* **2008**, *20*, 3942−3946.

(28) Raja, K.S.; Misra, M.; Gandhi, T. Effect of Water Content of Ethylene Glycol as Electrolyte for Synthesis of Ordered Titania Nanotubes. *Electrochem. Commun.* **2007**, *9*, 1069−1076.
(29) Macak, J. M.; Albu, S.; Kim, D. H.; Paramasivam, I.; Aldabergerova, S.; Schmuki, P. Multilayer TiO_2−Nanotube Formation by Two-Step Anodization. *Electrochem. Solid-State Lett.* **2007**, *10*, K28−K31.
(30) Chun, W.J.; Ishikawa, A.; Fujisawa, H.; Takata, T.; Kondo, J.N.; Hara, M.; Kawai, M.; Matsumoto, Y.; Domen, K. Conduction and Valence Band Positions of Ta_2O_5, TaON, and Ta_3N_5 by UPS and Electrochemical Methods. *J. Phys. Chem. B* **2003**, *107*, 1798−1803.
(31) Yang, X.; Li, C.; Yang, B.; Wang, W.; Qiam, Y. Optical Properties of Titanium Oxynitride Nanocrystals Synthesized via a Thermal Liquid_Solid Metathesis Reaction. *Chem. Phys. Lett.* **2004**, *383*, 502−506.
(32) Chan, M. H.; Lu, F. H. X-ray Photoelectron Spectroscopy Analyses of Titanium Oxynitride Films Prepared by Magnetron Sputtering Using Air/Ar Mixtures. *Thin Solid Films* **2009**, *517*, 5006−5009.
(33) Strydom, I. L.; Hofmann, S. The Contribution of Characteristic Energy Losses in the Core-Level X-ray Photoelectron Spectroscopy Peaks of TiN and (Ti, Al) N Studied by Electron Energy Loss Spectroscopy and X-ray Photoelectron Spectroscopy. *J. Electron Spectrosc. Relat. Phenom.* **1991**, *56*, 85−103.
(34) Mi, L.; Xu, P.; Wang, P.N. Experimental Study on the Bandgap Narrowings of TiO_2 Films Calcined under N_2 or NH_3 Atmosphere. *Appl. Surf. Sci.* **2008**, *255*, 2574−2580.
(35) Saha, N. C.; Tompkins, H.G. Titanium Nitride Oxidation Chemistry: An X-ray Photoelectron Spectroscopy Study. *J. Appl. Phys.* **1992**, *72*, 3072.
(36) Higashi, M.; Domen, K.; Abe, R. Highly Stable Water Splitting on Oxynitride TaON Photoanode System under Visible Light Irradiation. *J. Am. Chem. Soc.* **2012**, *134*, 6968−6971.
(37) Shvets, V.A.; Aliev, V. Sh.; Gritsenko, D.V.; Shaimeev, S.S.; Fedosenko, E.V.; Rykhlitski, S.V.; Atuchin, V.V.; Gritsenko, V.A.; Tapilin, V.M.; Wong, H. Electronic Structure and Charge Transport Properties of Amorphous Ta_2O_5 Films. *J. Non-Cryst. Solids* **2008**, *354*, 3025−3033.
(38) Lai, B.C.; Kung, N.; Lee, J. Y. A Study on the Capacitance−Voltage Characteristics of Metal-Ta_2O_5-Silicon Capacitors for Very Large Scale Integration Metal-Oxide-Semiconductor Gate Oxide Applications. *J. Appl. Phys.* **1999**, *85*, 4087−4090.
(39) Zhang, F.; Yamakata, A.; Maeda, K.; Moriya, Y.; Takata, T.; Kubota, J.; Teshima, K.; Oishi, S.; Domen, K. Cobalt-Modified Porous Single-Crystalline $LaTiO_2N$ for Highly Efficient Water Oxidation under Visible Light. *J. Am. Chem. Soc.* **2012**, *134*, 8348−8351.
(40) Maeda, K.; Terashima, H.; Kase, K.; Higashi, M.; Tabata, M.; Domen, K. Surface Modification of TaON with Monoclinic ZrO_2 to Produce a Composite Photocatalyst with Enhanced Hydrogen Evolution Activity under Visible Light. *Bull. Chem. Soc. Jpn.* **2008**, *81*, 927−937.
(41) Nakamura, R.; Tanaka, T.; Nakato, Y. Mechanism for Visible Light Responses in Anodic Photocurrents at N-Doped TiO_2 Film Electrodes. *J. Phys. Chem. B* **2004**, *108*, 10617−10620.
(42) Nah, Y.C.; Paramasivam, I.; Hahn, R.; Shrestha, N.K.; Schmuki, P. Nitrogen Doping of Nanoporous WO_3 Layers by NH_3 Treatment for Increased Visible Light Photoresponse. *Nanotechnology* **2010**, *21*, 105704.
(43) Ruff, T.; Hahn, R.; Killiana, M.S.; Asohb, H.; Schmuki, P. Visible Light Photoresponse From N-doped Anodic Niobium Oxide After Annealing in Ammonia Atmosphere. *Electrochim. Acta* **2012**, *62*, 402−407.